Nuclear Engineering and Technology 49 (2017) 825e837

Contents lists available at ScienceDirect

Nuclear Engineering and Technology

journal homepage: www.elsevier.com/locate/net

Original Article

Design response spectra-compliant real and synthetic GMS for seismic analysis of seismically isolated nuclear reactor containment building

Ahmer Ali [a], Nadin Abu-Hayah [b], Dookie Kim [b, *], Sung Gook Cho [c]

[a] ENVICO Consultants Co. Ltd., Songpa-gu, Seoul, 05718, Republic of Korea
[b] Civil and Environmental Engineering, Kunsan National University, Daehak-ro, Gunsan-si, Jeollabuk-do, 558, Republic of Korea
[c] Innose Tech Co., Ltd., Incheon, 406-840, Republic of Korea

a r t i c l e i n f o

Article history:
Received 3 May 2016
Received in revised form
1 February 2017
Accepted 8 February 2017
Available online 7 March 2017

Keywords:
ARMA Modeling
Base Isolation
Generation
Long-Period Motions
Nuclear Power Plants
Seismic Response
Tohoku
Record Selection

a b s t r a c t

Due to the severe impacts of recent earthquakes, the use of seismic isolation is paramount for the safety of nuclear structures. The diversity observed in seismic events demands ongoing research to analyze the devastating attributes involved, and hence to enhance the sustainability of base-isolated nuclear power plants. This study reports the seismic performance of a seismically-isolated nuclear reactor containment building (NRCB) under strong short-period ground motions (SPGMs) and long-period ground motions (LPGMs). The United States Nuclear Regulatory Commission-based design response spectrum for the seismic design of nuclear power plants is stipulated as the reference spectrum for ground motion selection. Within the period range(s) of interest, the spectral matching of selected records with the target spectrum is ensured using the spectral-compatibility approach. NRC-compliant SPGMs and LPGMs from the mega-thrust Tohoku earthquake are used to obtain the structural response of the base-isolated NRCB. To account for the lack of earthquakes in low-to-moderate seismicity zones and the gap in the artificial synthesis of long-period records, wavelet-decomposition based autoregressive moving average modeling for artificial generation of real ground motions is performed. Based on analysis results from real and simulated SPGMs versus LPGMs, the performance of NRCBs is discussed with suggestions for future research and seismic provisions.

1. Introduction

In light of recent earthquake events of the past decade, it can be said that earthquake-resistant designs seem to lack robustness against long-period excitations, raising safety concerns about civil infrastructure in terms of the development level of a nation as well as about nuclear-related facilities that empower the energy needs of this development. Stochastic models are used to quantify the extent of earthquakes in terms of the magnitude, path, site response, etc. These models are based on our knowledge of past experience and scientific predictions; however, the true nature of the seismic uncertainties is revealed with a future event itself [1].

In this context, the devastating hit of the Tohoku earthquake [magnitude (M) = 9.0], which occurred off the Pacific coast of Japan on March 11, 2011, caused extreme disasters due to high tsunami waves and low-frequency shakes. Such subduction zone earthquakes produce long-period, long-duration waves at larger distances from the rupture zone and tend to cause structures to resonate with lengthened modes of vibration for longer durations, leading to substantially severe structural damage and the imposition of stability hazards. In this regard, uncertainty in the impact of such ground motions and their effects on structural behavior have been taken up as an important issue. Therefore, a stochastic approach for the attenuation and simulation of acceleration records for dynamic analysis and site-specific hazard evaluation has been practiced for years. However, a limited number of studies have been carried out on the categorization, selection, and generation of seismic records with considerable long-period character; also, the dynamic behavior of civil and safety-related structures is vulnerable to excitations of such nature. Therefore, despite the collection of nuclear power plant (NPP)-specific studies, the present study also benefits from literature reported on the behavior of general long-period structures to determine the sensitivity of the subject.

Takewaki [2] and Takewaki et al [3] studied the severe aspects of the devastating Tohoku earthquake and reported the presence of

* Corresponding author.
E-mail address: kim2kie@kunsan.ac.kr (D. Kim).

http://dx.doi.org/10.1016/j.net.2017.02.006

fairly significant long-period wave components in the velocity and earthquake input energy spectra. It was observed that tall buildings were seismically affected by the low-frequency shakes, while at short-periods, the vibrations were effectively mitigated by the hard-rubber dampers. Furumura et al [4] compared the high-frequency content and long-period character of the Tohoku records (M = 9.0) with those of past destructive events like the 1995 Kobe earthquake (M = 7.3), the 2004 SE Off-Kii Peninsula earthquake (M = 7.4), the 2004 Mid-Niigata (M = 6.8) earthquake, and the 1994 Tonankai earthquake (M = 8), reporting the significance of the Tohoku earthquake's anomalous strong ground motions. Ali et al [5] performed incremental nonlinear dynamic analysis of Korean NPPs and reported higher probability of failure when those structures are exposed to long-period ground motions (LPGMs). Araki et al [6] examined the dynamic instability in high-rise steel moment resisting frames subjected to a pair of strong LPGMs. The drifting trend was found to be prominent in the lower stories when the natural periods of the structures were close to the dominant periods of the seismic inputs. Moreover, the drifting either led to residual inter story drift ratio of over 0.01, or to collapse corresponding to smaller design base shear. In an effort to suggest revisions in the seismic design standards of China, Xiang and Li [7] analyzed and acknowledged the attributes of long-period spectral components in United States-based records by grouping the horizontal motions, considering different sites and statistically determining the spectral corner periods with respect to the Chinese design spectrum.

Another important factor is to quantify whether a particular seismic source is capable of producing earthquakes of such higher magnitude; such a factor might be geologically debatable for Korean NPP sites as the zone can be realized as of only moderate seismicity. However, given the unpredictability of natural forces in the past, it is of interest to investigate the dynamic performance of a Korean nuclear reactor containment building (NRCB) against such strong seismic loads. In addition, the absence of a domestic earthquake database requires the use of a foreign seismic bin, which provides suites of appropriate records. If the appropriate recorded time-histories are unavailable, the gap can be filled using simulated time-histories [8,9].

The conventional properties of earthquakes, such as amplitude, frequency, duration, etc., are not considered sufficient to affect the structural seismic response in the recently reported studies. Therefore, it is proposed that we consider the nonstationarity in amplitude and the frequency content of a ground motion to significantly capture the true response. These nonstationary properties are described and introduced by computing the time varying spectrum of an earthquake record, using time-varying autoregressive moving average (ARMA) models [10,11]. In this framework, Conte et al [12] presented discrete time-varying ARMA models as a realization of real time histories and to generate nonstationary seismic motions. The nonstationarity both in amplitude and frequency were considered in the model along with Kalman filtering for the estimation of the time varying parameters. Also, Dong et al [13,14] proposed time varying and vector ARMA models to simulate a set of ground motions in the time and frequency domains. The proposed method utilized a Kalman filter to estimate the time varying parameters of the ARMA model; results showed good agreement between the actual and the synthesized ground motions. Mobarakeh et al [15] used a simplified time invariant ARMA (2, 1) model to reproduce the nonstationary amplitude and the frequency content of the acceleration record. Popescu and Demetriu [16] presented parametric ARMA models to analyze and simulate strong earthquake motions. The results were found to be promising and it is suggested that they can be utilized in the design of engineering structures.

Hence, the objective of this study is to investigate the influence of LPGMs on the seismic response of a base-isolated NRCB. For dynamic analysis, the selection of NRC-compliant records from the Tohoku earthquake is presented, ensuring the spectral compatibility within the period range(s) of interest. Since there lies a gap in the simulation of LPGMs, a method is proposed to simulate the preselected LPGMs and short-period ground motions (SPGMs). The comparatively substantial level of performance is discussed in terms of the lateral displacement, shear forces, and energy dissipation.

2. NRCB

2.1. Structural model

Using the lumped mass approach, the structural model of the seismically-isolated NRCB is converted into an equivalent stick model. Along the elevation of 65.4 m, the superstructure of the NRCB is divided into 13 segments, hereinafter referred to as "element(s)", as shown in Fig. 1. The physical characteristics have been primarily extracted in terms of translational and rotational mass, geometric and polar moment of inertia, pertaining to nodes of each element, respectively. The object-oriented software framework, Open System for Earthquake Engineering Simulations (OpenSees), is used to model the isolated NRCB [17]. The finite-element model contains a total of 15 nodes and 14 elements; the first element reflects the base isolation and the remaining 13 elements represent the superstructure, which is modeled using the command "element elasticBeamColumn". The elasticBeamColumn element is dimension-dependent and requires the cross-sectional area, the Young's and shear moduli moment of inertia, element mass per unit length, etc., to simulate the structural behavior. The use of elemental mass/density is optional (default = 0.0) and does not affect the structural response because the stiffness and the mass characteristics of all elements and the relevant nodes are explicitly input in the analysis model. Hence, the mean geometric area and the moment of inertia associated with each element are 168.69 m^2 and 3.98 $\times$ 10^4 m^2, respectively, where the mean translation mass of each node is 1994.60 kN.s^2/m. The nodal mass and element stiffness details of each node and element are illustrated in Table 1 [18].

2.2. Base isolation

2.2.1. Finite element modeling

Using the uniaxial material constitutive law, the base-isolation is modeled using a particular element object in OpenSees, especially dedicated to simulate the bilinear shear and force-deformation behavior of a typical elastomeric lead rubber bearing (LRB). Using the command "element elastomericBearingPlasticity", the element is defined between two nodes having zero-length or any appropriate bearing height. The two nodes of the elastomeric zero-length element, used herein, are rigidly connected, having a shear hinge at the distance sDRatio.L from the bottom node. The term L refers to the element length, which is inapplicable in the case of a "zeroLength" element. Thus, the value of the factor sDRatio = 0.5 is used to deploy the shear hinge at the element center and, thus, ensure equal distribution of forces and P-delta moments between the two nodes. The functional schematics of the zero-length elastomeric bearing and the bilinear hysteretic shear-deformation law are shown in Fig. 2.

As can be observed in Fig. 2, the bilinear shear-deformation model follows the use of the isolator's yield strength F_y, the initial yield stiffness K_u in the local shear direction and the post-yield stiffness K_d, which represents the extent of linear hardening. The

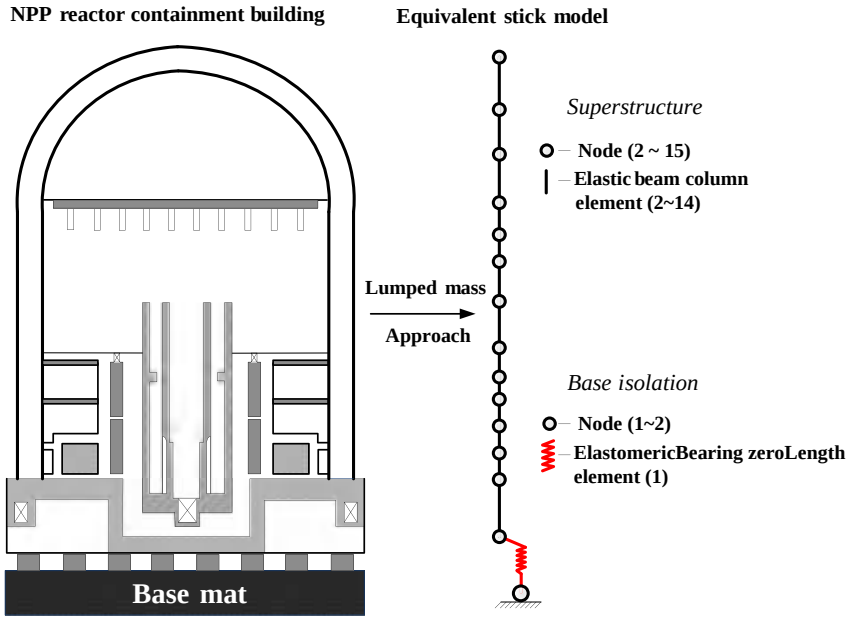

Fig. 1. Lumped mass model of the base-isolated nuclear reactor containment building (NRCB).

Table 1
Mass and stiffness details [base-isolated nuclear reactor containment building (NRCB)].

Node No.	Elevation (m)	Translational mass (kN.s^2/m)	Rotational mass ($\times 10^4$ kN.m.s^2)		Elem. No.	Moment of inertia		Remarks
						Geometric	Polar	
		X=Y=Z	XX=YY	ZZ		($\times 10^4$ m^4)		
1	0.000	d	d	d	d	d	d	
2	0.000	1074.058	27.417	54.832	1	d	d	Elastomeric bearing
3	5.182	1914.917	48.110	95.494	2	4.398	8.795	Elastic beam-column element
4	8.534	1390.876	35.435	70.870	3	4.398	8.795	
5	11.89	1648.591	36.519	75.865	4	4.398	8.795	
6	14.94	1264.499	32.208	64.417	5	4.398	8.795	
7	17.98	1328.563	41.545	87.118	6	4.398	8.795	
8	21.34	2086.095	53.250	10.650	7	4.398	8.795	
9	28.04	3603.493	92.379	18.476	8	4.398	8.795	
10	38.71	2844.794	72.950	14.590	9	4.398	8.795	
11	41.76	2004.081	40.060	82.248	10	4.398	8.795	
12	44.81	2009.918	49.893	98.454	11	4.398	8.795	
13	52.43	2756.359	62.581	12.249	12	3.753	7.506	
14	60.05	2756.359	39.340	75.932	13	2.856	5.713	
15	65.84	1241.733	5.8605	11.371	14	1.152	23.04	

* Young's Modulus = 29.16 GPa. Shear Modulus = 12.46 GPa.

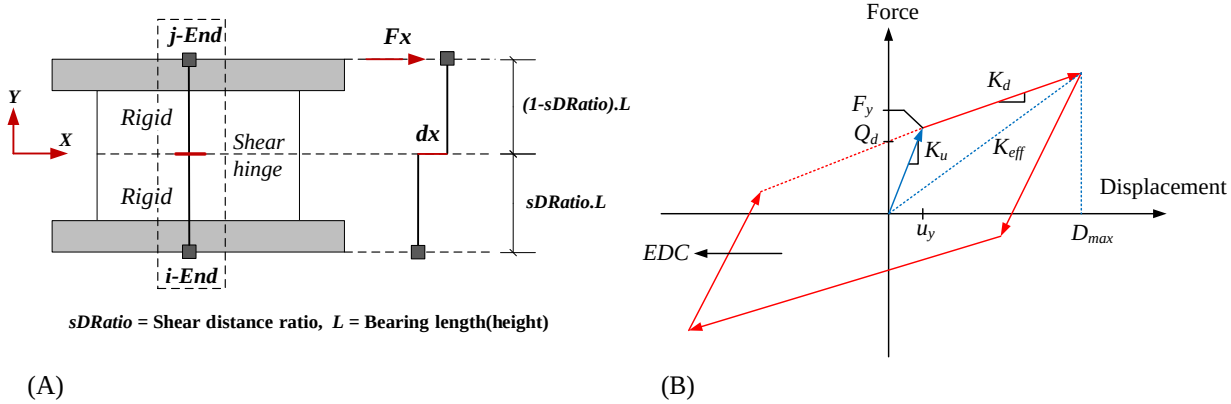

Fig. 2. (A) ElastomericBearing Element in Opensees. (B) Bilinear force-deformation relationship.

Fig. 3. Compression-shear load equipment.

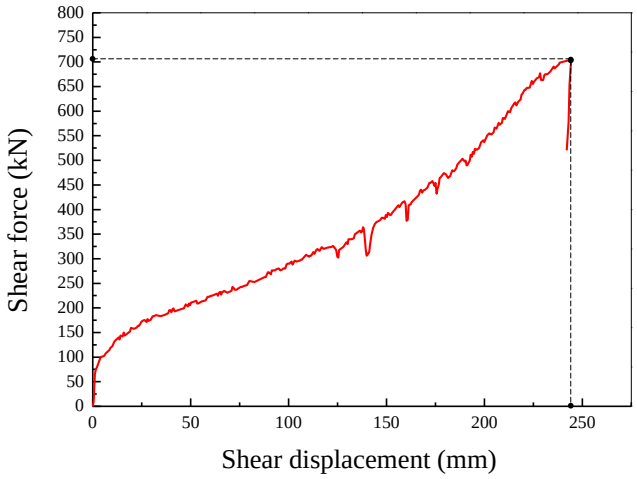

Fig. 4. Shear load-displacement curve.

Table 2
Capacity of the lead rubber bearing (LRB) test equipment.

	Max. load (kN)	Max. displacement (mm)	Max. velocity
Vertical capacity	30,000	150	1 (mm/sec)
Horizontal capacity	± 5000	± 1,000	20 (mm/sec)
Moment capacity	± 500	± 100	± 1000 (kN.m)

mechanical characteristics of the LRB isolator are obtained from the experimental studies explained in the section below.

2.2.2. Test program

The factors governing the behavior of elastomeric bearing in the FE modeling were extracted from the results of a test performed on the LRB isolators, complimented by the design guidelines provided by Naeim [8] and Naeim and Kelly [9]. The compression-shear test setup followed the specifications of ISO 22762:2010, 6.2.2 and the whole test program was executed by the Korean Testing and Research Institute in association with UNISON, Korea [19,20]. Fig. 3 and Table 2 show the test equipment and its horizontal and vertical load capacity, respectively.

The geometrical specifications of the LRB isolator test specimen are presented in Table 3. A compressive load of 6,600 kN, designed at the target shear strain of 1.5 and design displacement of approximately 200 mm, was applied uniformly to the isolator to maintain the design in-plane pressure. Fig. 4 shows the ultimate shear displacement graph, marking the breaking load at 705.1 kN. The summary of the obtained physical strength and breakage parameters of the isolator are illustrated in Table 4. For simplicity, the properties of a total number of 16 isolators were integrated and used as a single bilinear elastomeric zero-length element in the NRCB's finite element model.

2.2.3. Model validation

Prior to dynamic analysis, primitive validation of the FE model is performed by modal analysis to obtain the fundamental period and mode shapes of the isolated nuclear containment. The acquired first period of vibration (i.e., 2.02 seconds) verifies the accuracy of the FE plant model by complying with the design target period, i.e., 2.00 seconds, for which the required stiffness was obtained using Eq. (1), as follows [8,9]:

$$K_T = 2\pi\left(\frac{M}{T_H}\right)^2 \quad (1)$$

$$K_H = K_{T=n} \quad \therefore n = \text{number of isolators} \quad (2)$$

where M, K_T, K_H and T_H are the total mass, total horizontal stiffness, horizontal stiffness of one isolator, and target fundamental period of the isolated structure, respectively.

3. Selection of earthquake records

3.1. Target spectrum

The selection of ground motions is of crucial importance in dynamic, linear or nonlinear response analysis of structures, as it controls the outcomes and performance levels for which the structure ought to be designed. Since safety-related nuclear facilities in Korea are known to be initially designed in compliance with the seismic design response spectra reported in Regulatory Guide 1.60 of the United States Nuclear Regulatory Commission [5,18,21], the 5% damped NRC response spectrum is set as the target spectrum for ground motion selection.

The plot of the 5% damped NRC spectrum, a simplified illustration of the four control points governing the spectrum and its values, is shown in Fig. 5 and Table 5. For details on spectra other than the 5% damping spectra, refer to [21].

3.2. Strong ground motion database

Once the target spectrum is identified, the earthquake records can be selected from any available extensive repository or database

Table 3
Geometrical specifications of lead rubber bearing (LRB) isolator.

Bearing diameter (mm)	Lead core diameter (mm)	Rubber thickness (mm)	No. of rubber layers	Insert plate thickness (mm)	No. of insert plates	End plate thickness (mm)
1,003	315	9.5	12	4	11	20

Table 4
Mechanical characteristics of lead rubber bearing (LRB) isolator.

Horizontal stiffness K_H (kN/mm)	Post-yield stiffness K_d (kN/mm)	Characteristic strength K_d (kN)	Equivalent damping ratio	Breaking strain (mm)	Shear load at break (kN)
16.91	5.22	653.7	41.41%	244.6	705.1

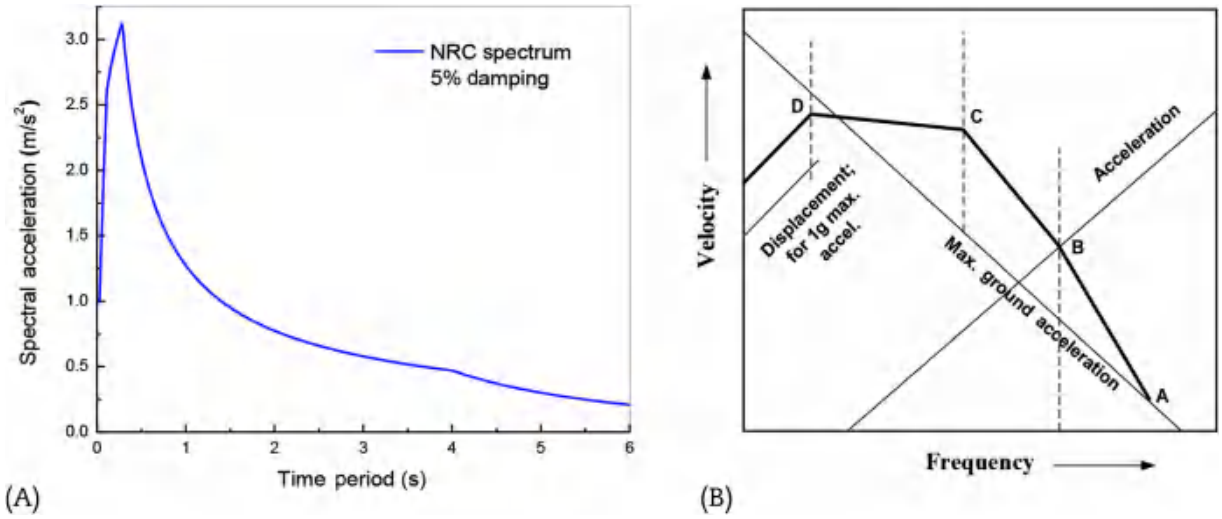

Fig. 5. (A) Nuclear reactor containment (NRC) design response spectrum. (B) Four control points e NRC.

Table 5
Relative amplification factors for control points e for horizontal design response spectra (DRS).

Critical damping value (%)	Amplification factor values for relevant control points			
	Acceleration			Displacement
	A (33 cps)	B (9 cps)	C (2.5 cps)	D (0.25 cps)
5.0	1.0	2.61	3.31	2.05

of ground motions. In this context, the idea of spectrum compatibility is often adopted and proposed for earthquake record selection using several seismic codes, and utilized in the framework of force-based and performance-based design [22]. Since Korea does not have any bin of recorded motions, the Japanese strong motion databases K-NET and Kik-NET (http://www.kyoshin.bosai.go.jp) are used for downloading and selecting the motions to match the target spectrum. The infamous event of Tohoku, 2011, has been reported to have undoubtedly devastated several moderate-to-long-period structures, including the nuclear facilities in Japan [2,3], clearly surpassing the seismic standards in place. The ground motions of this subduction zone earthquake are specifically focused on for selection, due to this earthquake's tendency to produce long-period long-duration waves at larger distances from the rupture zone, and hence substantially causing resonating in long-period structures, such as skyscrapers, high-rises, NPPs, etc., and causing severe damage.

3.3. Spectral matching

For spectral matching, decision-making in fixing the period range of interest is of high significance. Regardless of the structure type, the first/fundamental period of vibration (T_1) is greatly important for engineers; however, ideally, this range should encompass all the periods to which the structural response is sensitive. ASCE 7-05 [23] suggests from $0.2T_1$ to $1.5T_1$ as an effective period range; however, nonlinear structures with effectively lengthened T_1- base-isolated NRCB, herein, are found to be sensitive to response spectra for periods greater than $1.5T_1$ [24].

In this study, a dual band of periods is chosen to match the target spectrum with the selected records. The first band (Band 1) involves the periods associated with the acceleration sensitive domain, i.e., the flat region of the spectra, referring to the seismic effect at vibration modes of high-order. Band 1 entails the period range of 0.1 seconds to T_2, where T_2 is pertinent to the control point C in Fig. 5B and Table 5, i.e., 0.4 seconds. The second band (Band 2) constitutes the fundamental period of the seismically isolated NRCB, as it controls the total response of the structure [5,25]. Since modal analysis has revealed a lengthened first period of the isolated containment, i.e., 2.02 seconds, signifying its sensitivity to longer periods, a period range of $T_1 \pm 0.5T_1$ is decided on for Band 2.

With the period range of interest decided, a large number of records from Tohoku are assessed to identify the most closely matching motions with the target spectral shapes within the given bands of periods. The similarity between the target spectrum and selected records is determined by checking the sum of the root mean square error (E_{rms}) of the spectral accelerations at any period range $S_a(T_i)$, as follows [5,26]:

$$E_{rms} = \frac{1}{N_i}\sqrt{\sum_{i=1}^{N}\left(\frac{S_a(T_i) - S_a^T(T_i)}{S_a^T(T_i)}\right)^2} \quad (3)$$

Here, $S_a(T_i)$ is the spectral acceleration of the record, $S_a^T(T)$ is the target spectral acceleration at period T_i and N_i is the total number of periods in a specified band. According to Eq. (3), the records with the smallest E_{rms} values are selected for SPGMs; however, an extra margin of about 10~15% is allowed specifically in Band 2 for the selection of LPGMs. It is thought that perhaps the NRC spectrum does not reflect the characteristics of the long-period records and, thus, referring to the natural period of the structure, real spectrum matching in Band 2 was chosen as a selection criterion. It is believed that the records complying with Eq. (3) and complemented by this extra allowance shall provide a reasonable representation of the long-period character and its effects on the structure response.

Fig. 6 demonstrates the selection of earthquake records in accordance with the aforementioned dual band of periods.

3.4. Number of records

The minimum number of records required for the engineering analysis of the structure differs for various codes. According to ASCE 4-98, the minimum number of records is decided on depending on the type of response required, e.g., to compute the maximum response, at least three to six recordings or a minimum of one

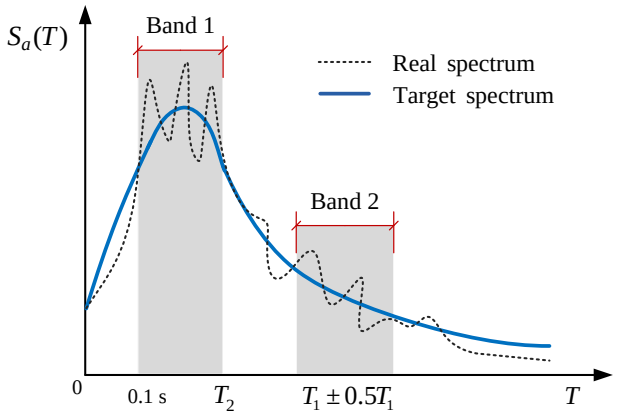

Fig. 6. Selection and spectral matching of earthquake records w.r.t dual band of periods.

record is allowable unless the structure is vulnerable to long-period motions. Moreover, engineers are allowed to conclude that the behavior is a mean structural response if at least seven ground motions are used for the structural analysis, as was adopted in the present study [21,27]. The set of seven records, for short- and long-period motion categories, are selected using the criterion discussed earlier and shown in Fig. 7 below.

4. Simulation of earthquake records

For each set of selected records, an equivalent ground motion is simulated for the time history dynamic analyses using the parametric time varying ARMA (TVARMA) modeling. Moreover, wavelet transform based decomposition is applied to divide the seismic signal into two parts, i.e., of high and low frequency. This purpose is achieved by passing the signal through low pass and high pass filters. The low pass filter eliminates the high frequency bands of the original signal and returns its approximated version, whereas the high pass filter removes the low frequency content and yields an approximation of the original signal. The decomposition can be performed at multiple levels by repeating the process and using the low pass filtered data from the preceding step [28e30]. Since the influence of the long-period component on the structural response is desired, using ARMA modeling, only the high frequency content of the LPGMs is synthesized and then adjoined with the original low-frequency content to obtain artificial LPGMs. However, for SPGMs, wavelet transform-decomposition is avoided and the records are processed through the parametric TVARMA (p, q) model as a realization of a nonstationary random process, expressed as follows [10e13,31,32]:

$$y_k - f_{1;k}y_{k-1} - \ldots - f_{p;k}y_{k-p} = e_k - q_{1;k}e_{k-1} - \ldots - q_{q;k}e_{k-q} \quad (4)$$

Here y_k, e_k and $s^2_{e;k}$ are the earthquake ground motion, the Gaussian white noise $[(e_k \sim N(0; s^2_{e;k}))]$ and the envelope function of the noise and represented in nonstationarity in amplitude, respectively. The variables $f_{i;k}(i = 1; 2; \ldots; p)$ and $q_{i;k}(i = 1; 2; \ldots; q)$ denote the time varying AR and MA coefficients, respectively, and account for the nonstationarity in the frequency content. The subscript k denotes the instant t=kDt, where Dt is the sampling time. The steps involved in the process are as follows:

(1) Order (p, q) selection of the TVARMA model: The process initiates with the selection of the model order because this value plays an important role in the estimation of the time varying spectrum. As mentioned earlier, the term "time varying" in ARMA modeling is related to nonstationarity in both frequency and amplitude; therefore, the order of the model should also be time varying, unlike time invariant models. However, to determine such a model order is known to be a tedious errand; thus, an optimized fixed model order can be selected through the time invariant ARMA model using the Akaike Information Criterion, given that the nonstationary spectral properties of the TVARMA model are well accounted for [11,33,34].

(2) State-space form of TVARMA model: Like many other dynamic models, the TVARMA model(p, q) can be written in state-space form as in Eqs. (5) and (6), which represent the sequential transition of the model (state) from one moment, i.e., first-order auto regression, to the other:

$$y_k = H_k^T X_k + e_k \quad (5)$$

$$X_k = X_{k-1} + V_{k-1}; \quad (6)$$

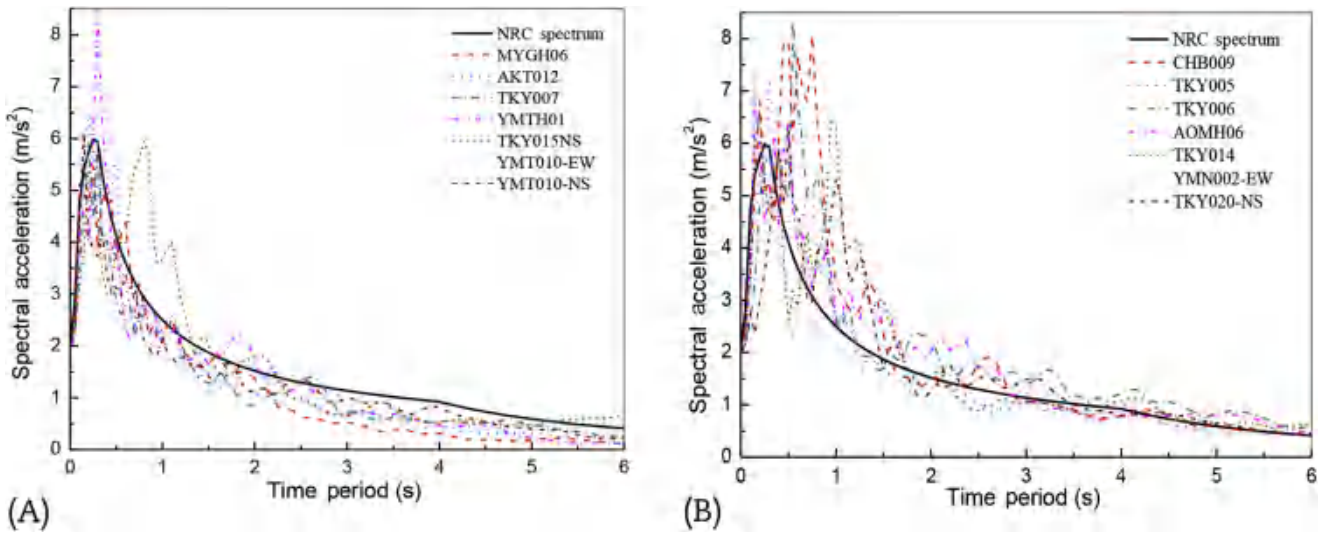

Fig. 7. Nuclear reactor containment (NRC) spectrum compatible spectra. (A) Short-period ground motions (SPGMs). (B) Long-period ground motions (LPGMs).

The goal behind a state-space representation is to obtain the dynamics of an observed vector y_k in terms of an unobserved vector X_k, called the state vector of the system. The predictions for y rely on $(y_k; y_{k-1}; \dots)$ through the present value of y_k [35].

Here, $H_k = [y_{k-1}; \dots; y_{k-p}; e_{k-1}; \dots; e_{k-q}]^T$ is called an observed/measurement vector, e_k, similar to that in Eq. (4), which refers to the measurement noise:

$X_k = [f_{1;k}; \dots; f_{p;k}; -q_{1;k}; \dots; -q_{q;k}]^T$ and $V_k = [\eta_{1;k}; \dots; \eta_{p+q;k}]^T$ is a Gaussian process using white noise with $V_k \sim N(0; Q_k)$ [11,12].

(3) Parameter estimation using a Kalman filter: The Kalman filter helps estimate the time varying parameters, and is referred to as a "state vector" X_k in the aforementioned state-space model. The iteration starts by constructing the first measurement vector H_0 using an initial p value of y_k and q value of zeros; H_0 is drawn based on the stationary time invariant ARMA model at initial values of y_k; covariance P_0 is taken as equal to Q_k. The Kalman recursive state-space estimation is formulated as follows [11,12]:

$$\widehat{P}_{k+1} = P_k + Q_{k+1}; \tag{7}$$

$$K_{k+1} = \widehat{P}_{k+1} H_{k+1}^T \left(H_{k+1}^T \widehat{P}_{k+1} H_{k+1} + s_{k+1}^2 \right)^{-1}; \tag{8}$$

$$X_{k+1} = X_k + K_{k+1} \left(y_{k+1} - H_{k+1}^T X_k \right) \tag{9}$$

$$P_{k+1} = \left(I - K_{k+1} H_{k+1}^T \right) \widehat{P}_{k+1} \tag{10}$$

Here, $\widehat{P}_{k+1}$ and P_{k+1} are the prediction and the posterior covariance of the state and K_{k+1} is the Kalman gain. The Kalman filter monitors the likelihood of the forecast by estimating e_{k+1}, which in state-space representation equals $y_{k+1} - H_{k+1}^T X_k$ and thus, Eq. (9) can be re-written as:

$$X_{k+1} = X_k + K_{k+1} e_{k+1} \tag{9a}$$

Q_k is the process noise covariance and shows the state's nonlinearity; referring to [11], its value is considered to be 10^{-4}I, where I is the unit matrix. Thus, all the state vectors are sequentially estimated and the iteration is successful when $s_k^2 = [(k-1), s_{k-1}^2 + e_k^2] = k < (s_k^2)_{limit}$, where after each iteration e_k^2 0 $\widehat{e}_k$ indicates the residue.

(4) Estimation of the time-varying spectrum: With the time varying parameters estimated, the time varying spectrum of the forecasted/simulated earthquake ground motions can be achieved using the following expression [11,12]:

$$p(f; k) = 2 s_k^2 \frac{\left| 1 - q_{1;k} e^{-i2pf\Delta t} - / - q_{q;k} e^{-i2pqf\Delta t} \right|^2}{\left| 1 - f_{1;k} e^{-i2pf\Delta t} - / - f_{p;k} e^{-i2ppf\Delta t} \right|} \Delta t \tag{11}$$

where f is frequency (Hz) and f 2 $[0; f_s/2]$ is the sampling frequency $(f_s) = 1/\Delta t$.

(5) Estimation of spectral error: The spectral compatibility of the simulated ground motion with the target spectrum is checked by comparing the relative error e_{rr} with the threshold error e_t, as follows:

$$e_{rr} = \sum_{k=1}^{n} \left| \frac{S_a(y_k) - S_a^T(y_k)}{S_a^T(y_k)} \right| \quad \therefore e_{rr} \le (e_t = 10 \sim 15\%) \tag{12}$$

If the error is more than the preset limit, the process is repeated, followed by the regeneration of the white noise, e_k, until the desired precision is achieved. Moreover, in order to obtain multiple ground motions, a counter to generate multiple e_k can be set.

As an application of the discussed technique, Fig. 8 shows the spectral comparison of the real and simulated SP and LPGM. For brevity, the mean of the real and simulated spectra is shown with the target spectrum in Fig. 8C; also, the spectral values $S_A(T_1)$ corresponding to the fundamental period of the isolated NRCB are marked. Furthermore, as a reliable reference to discuss the stability of the results, the difference in the average spectral ratio of the SPGMs and LPGMs, within Band 2, is calculated and found to be approximately 0.70 for both or real and simulated ground motions.

5. Analysis results

In order to assess the dynamic performance of the isolated NRCB, the real and artificial LPGMs and SPGMs, described in the earlier sections, are used as seismic inputs for the time history response analyses. The analysis is load controlled and follows the Newton-Beta algorithm for numerical integration; the seismic load is applied with a time increment of 0.01 seconds. The damping coefficients are calculated using Eq. 3.1-3 in ASCE 4-98, for which the first Rayleigh frequency is based on the first Eigen frequency of the system and the second Rayleigh frequency is pertinent to the zero-period acceleration frequency, i.e., taken as 38 Hz [27,36,37]. The results, recorded in terms of lateral nodal displacements, base and inter-story shear forces, hysteresis energy dissipation per each cycle of the acceleration histories, etc., are presented below.

5.1. Nodal displacements

Fig. 9 shows the lateral nodal displacements exhibited by the base-isolated NRCB, corresponding to each set of NRC compliant real SPGMs and LPGMs, with the record/station names given in the legends. It can be seen that the maximum displacement is recorded at the isolator, i.e., Node 2, followed by the gradual drift in the NRCB superstructure, which peaks at the top (Node 15). As the inter-story drift is considerably negligible, the discussion will mostly focus on Node 2. Moreover, it can be observed that the isolator displacement for SPGMs does not exceed the design displacement, which is also true for certain LPGMs, except for two records that show significant margins, which could possibly lead to skeptic regarding the observation pertaining to the selection of these records at lower frequencies. However, complying with the aforementioned ASCE regulations for the considered number of ground motions, the mean response is targeted to evaluate the seismic behavior. In addition, since this study aims at evaluating the relative impact of SPGMs and LPGMs, along with their simulated surrogates, on the seismic performance of the isolated NRCB, the mean (μ) results and probabilistic deviations (σ) for all categoric ground motions are graphically presented and tabulated. Fig. 9C shows the mean displacements μ_D corresponding to the real and simulated SPGMs and LPGMs. As expected, the SPGMs did not exceed the allowable isolator displacement, whereas the LPGMs nearly crossed the permissible limit and outweighed by over 35% the SPGMs. However, considering the probabilistic distribution with the obtained standard deviation σ_D, shown in Table 6, the response for the LPGMs seems to approach the isolator's breaking limit, while the SPGMs still lie within the allowable bounds. In cases of simulated ground motions, the mean

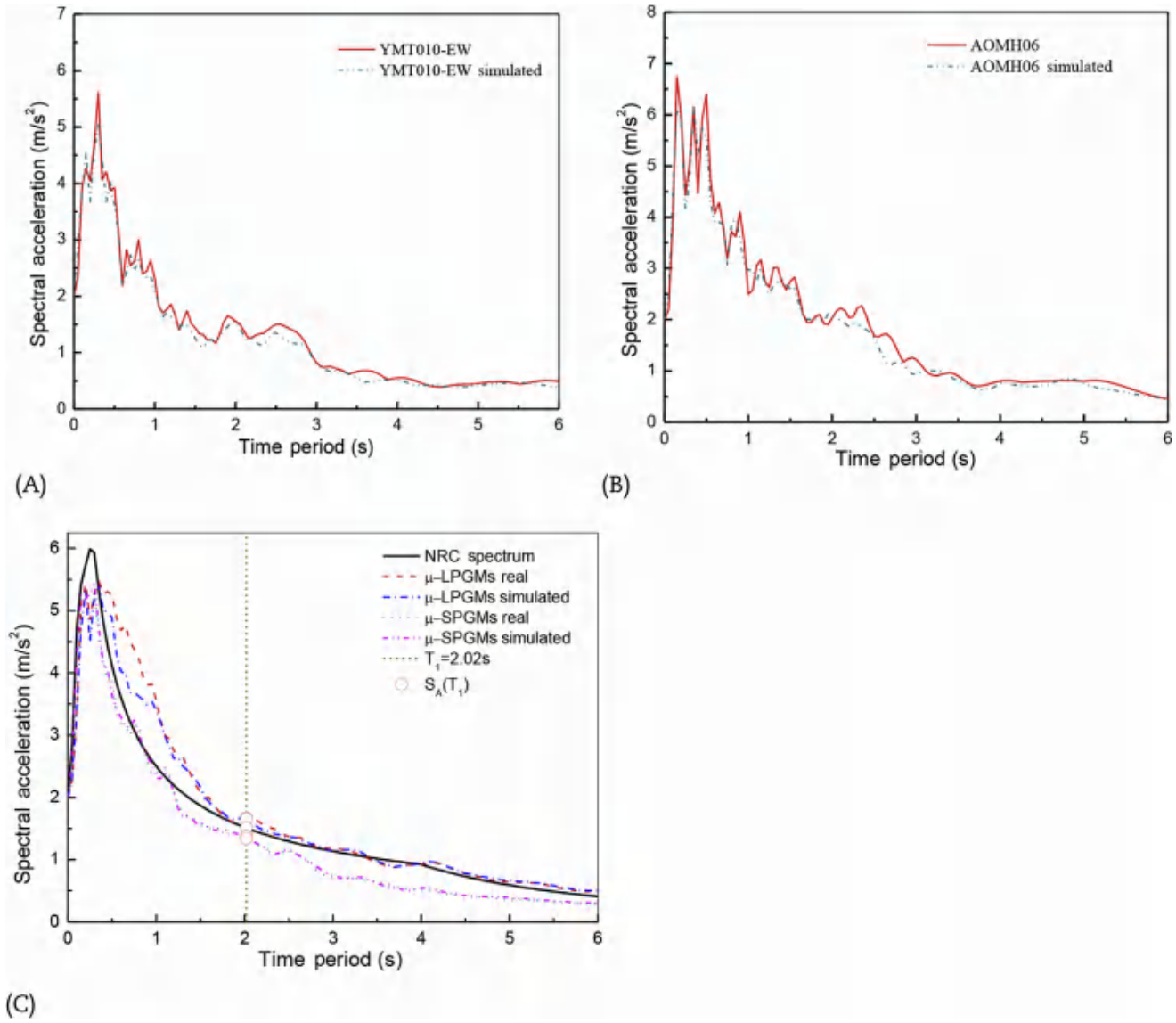

Fig. 8. (A) Real and simulated short-period ground motion (SPGM) spectra. (B) Real and simulated long-period ground motion (LPGM) spectra. (C) Mean SPGM and LPGM spectra.

isolator displacement m_D is overestimated by 5% and underestimated by 2.5% relative to the real SPGMs and LPGMs, respectively, with identical overall response deviating by over 35%. Hence, so far the results imply an onerous effect of the LPGMs on the safety of the seismically isolated NRCB; also, the m_D and s_D-values prominently signify the suitability of the simulated records for the performance analysis. The 35% deviation between the SPGM and the LPGM results can be explained by the aforementioned average spectral difference in Band 2 of the selected ground motions.

5.2. Base shear

Fig. 10 shows the maximum shear force for SPGMs and LPGMs along the elevation of the base-isolated NRCB model. The maximum shear force is achieved at the base, followed by the shear force at the isolator, which shows an insignificant difference; by contrast, the inter-story shear gradually decreases with the height due to the seismic isolation phenomenon. The plots of the mean shear forces m_F for both real and simulated ground motions are presented in Fig. 10C. The behavior is analogous to the nodal displacements, such that the mean base shear increased by over 35% for LPGMs as compared to SPGMs and shear forces under simulated records are 2.3% lower for LPGMs and 4.4% higher for SPGMs. Since the NRCB appeared to be credibly vulnerable to LPGMs, the impact shown in the LP-simulated records, considering the probabilistic distribution of the shear forces m_F, illustrated in Table 7, provides an important consideration.

5.3. Energy dissipation

The energy dissipation is computed using the cumulative trapezoidal numerical integration of the resisting force with respect to the associated displacement at Node 2 for each type and set of ground motions. The energy dissipation values, hereinafter also referred to as “hysteresis energy”, under the real SPGMs and LPGMs, are shown in Fig. 11A and 11B. A comparison of maximum hysteresis energy (E) for each ground motion, the maximum mean

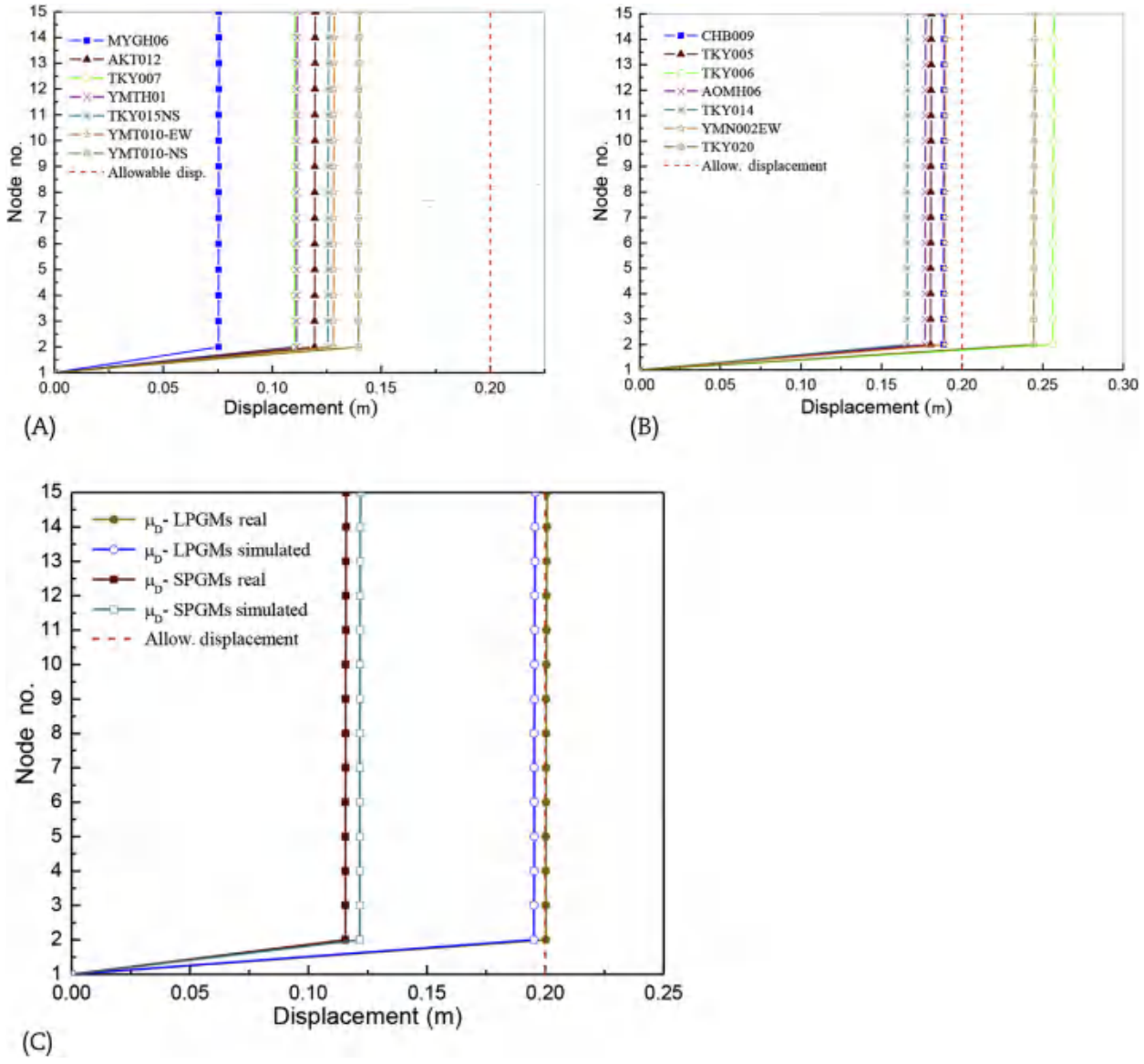

Fig. 9. (A) Displacement of real short-period ground motions (SPGMs). (B) Displacement of real long-period ground motions (LPGMs). (C) Mean displacement (μ_D).

Table 6
Mean displacement μ_D, comparison at Node 2 for short-period ground motions (SPGMs) and long-period ground motions LPGMs (m).

	SPGMs		LPGMs	
	Real	Simulated	Real	Simulated
μ_D	0.116	0.122	0.200	0.195
S_D	0.021	0.039	0.035	0.038

energy μ_E of each set of records and the standard deviation S_E of the maximum mean energy, is illustrated in Table 8. However, for brevity, the influence of the simulated records is shown only as mean plots, given in Fig. 11C. It can be seen that the maximum mean energy μ_E is dissipated at a level approximately 40% higher by the isolated structure when subjected to LPGMs. The initial rate of change of the energy is noticeable for SPGMs until around 105 seconds, the point at which nearly the same amount of energy is dissipated by all types of ground motions. Prior to 105 seconds, the simulated SPGMs have greater hysteresis energy, but beyond that point, the cumulative μ_E curve seems to converge with that of the real SPGMs at 150 seconds and utilizes almost the same amount of energy while maintaining the mild gradient until the end, at which point the simulated records surpass the real ground motions by 2.02%. However, in the case of LPGMs, the energy slope is low and mild until 85 seconds, from which point the gradient escalates sharply, crossing that of the SPGMs, until reaching 125 seconds. Beyond this time, the curve turns smoothly and less steep with gradual increase in μ_E. Although the value of μ_E for the LP-simulated records is higher at several instances over time, the value dropped slightly, by 0.1%, at the maximum time, i.e., at 285 seconds, in contrast to the real LPGMs.

In order to better understand the influence of LPGMs on the seismic performance of the base isolated NPP structure, the mean energy dissipation per cycle μ_{EDC} is computed using the scenario presented in Fig. 12 below. The change in energy is seen to be more pronounced at the steeper part of the curve; therefore, 5~95 % of E_{max} is assumed to effectively contribute in obtaining the value of

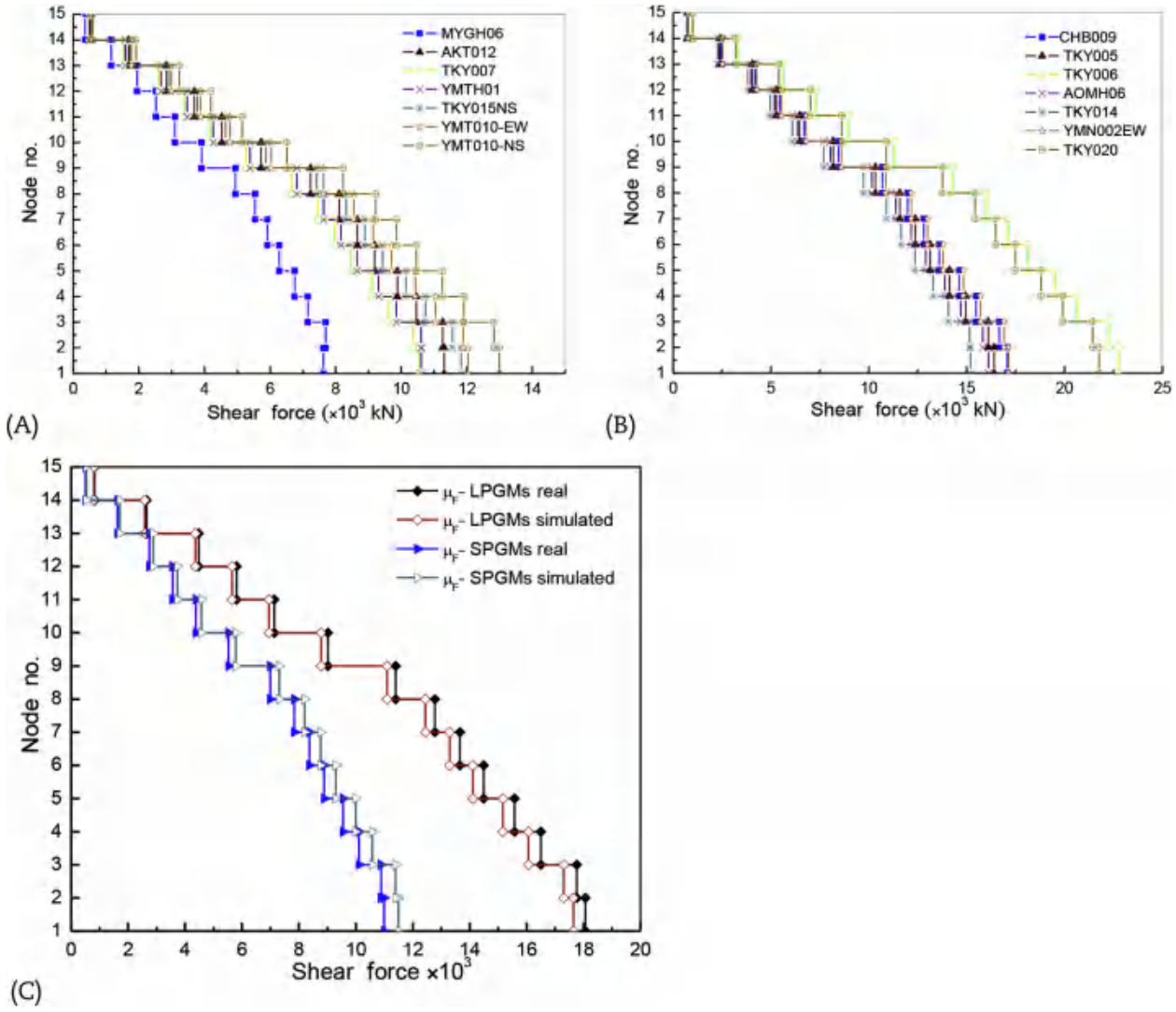

Fig. 10. (A) Maximum shear force for real short-period ground motions (SPGMs). (B) Maximum shear force for real long-period ground motions (LPGMs). (C) Mean shear force (m_F).

Table 7
Base Shear (× 10^3 kN) comparison for short-period ground motions (SPGMs) and long-period ground motions (LPGMs).

	SPGMs		LPGMs	
	Real	Simulated	Real	Simulated
m_F	10.991	11.500	18.062	17.646
s_F	1.711	3.245	2.951	3.155

m_{EDC} for each case of ground motions, using the expression also described in Eq. (13).

$$m_{EDC} = \frac{E_{95} - E_5}{N_z \left| \begin{matrix} t_2 = T_{95} \\ t_1 = T_5 \end{matrix} \right\rangle} \tag{13}$$

Here, $E_5 = 5\%(E_{max})$, $E_{95} = 95\%(E_{max})$ and N_Z are the number of cycles within T_5~T_{95}.

For better illustration, the results are compared in Table 9. The mean hysteresis energy per cycle m_{EDC} for LPGMs is computed and found to be around 48% higher than that value for SPGMs. Moreover, the value of m_{EDC} for the simulated SPGMs is 3.64% greater than that from the real records, whereas for LPGMs the difference is 0.11%. The amounts of deviation are acceptable, because the relative error e_{rr} is kept under 10~15% in the simulation of the artificial ground motions.

6. Conclusions

The influence of the strong ground motions of the Tohoku earthquake on the seismic response of a Korean nuclear facility is investigated. The focus is primarily put on the structural effects of long-period low-frequency records of the mega event, and a spectral compatibility based selection criterion is presented to allow a choice of long- and short-period time histories for transient dynamic analysis of a seismically isolated NRCB. The selection is performed pertaining to the acceleration sensitive region and the fundamental period of the structure, both of which are in vulnerable period ranges for the structural response. Spectral precision within these periods of interest is attained by estimating the sum of the squared roots using Eq. (3). Seismic analysis is also provided for the artificial nonstationary records, simulated by wavelet decomposition based ARMA modeling of the selected time histories. The performance level of the NRCB is presented according to the

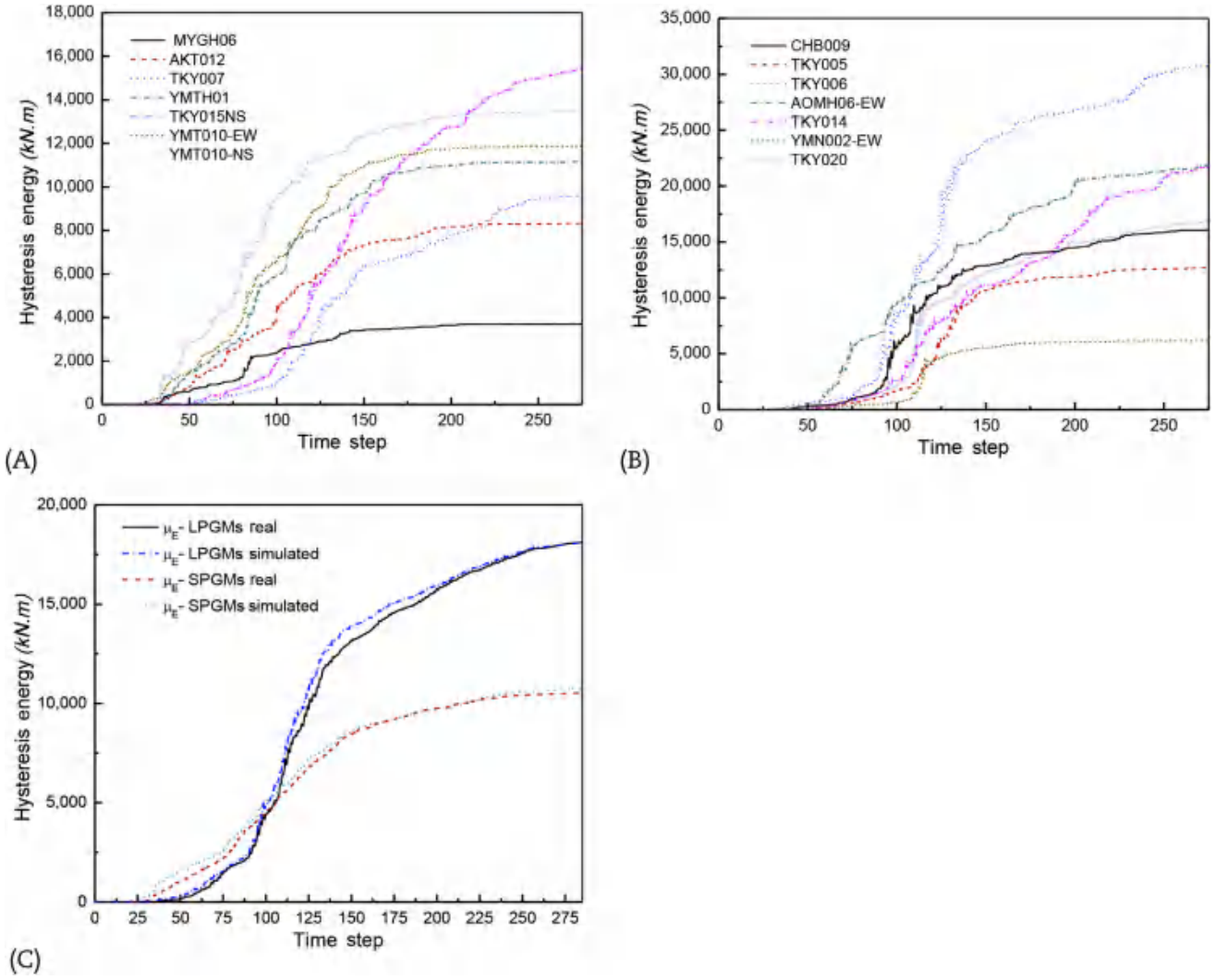

Fig. 11. (A) Hysteresis energy for real short-period ground motions (SPGMs). (B) Hysteresis energy for real long-period ground motions (LPGMs). (C) Mean hysteresis energy (m_E).

Table 8
Comparison of maximum hysteresis energy at Node 2 (KN.m).

SPGMs			LPGMs		
	Real	Simulated		Real	Simulated
Record name	Max. energy		Record name	Max. energy	
MYGH06NS2	3,700.132	3,089.784	CHB009NS	16,108.252	22,666.193
AKT012EW	8,324.327	6,190.416	TKY005NS	12,696.891	13,665.865
TKY007NS	9,644.169	16,367.640	TKY006NS	31,028.313	29,894.889
YMTH01NS2	11,170.43	7,130.955	AOMH06EW2	21,898.200	17,098.649
TKY015NS	15,477.87	17,317.34	TKY014NS	21,828.629	21,391.842
YMT010EW	11,867.61	11,153.96	YMN002EW	6,146.0622	8,799.8121
YMT010NS	13,464.75	13,911.26	TKY020NS	17,057.079	13,130.887
m_E	10,521.330	10,737.340	m_E	18,109.061	18,092.591
$\pm S_E$	3,820.770	5,437.670	$\pm S_E$	7,880.510	7,102.291

isolator displacement, base shear, hysteresis energy and energy dissipation per cycle. The overall response is analyzed using mean m-values for each ground motion category, complying with the ASCE regulations for the selected number of records. Hence, it can be concluded that: (1) the selected set of LPGMs increased the mean isolator displacement, base shear, and hysteresis energy by 35~40% as compared to SPGMs; this result is noticeably compatible with the average spectral difference (i.e., 0.7 approx.) in Band 2 of the selected SPGMs and LPGMs; (2) the mean isolator displacements m_D for SPGMs are less than the allowable design displacement. In the case of LPGMs, calculated mean displacements are nearly equal to the allowable design displacements; (3) in the case of hysteresis energy m_E, a similar amount of mean energy is dissipated at 105 seconds for both categories of records. Afterwards, the

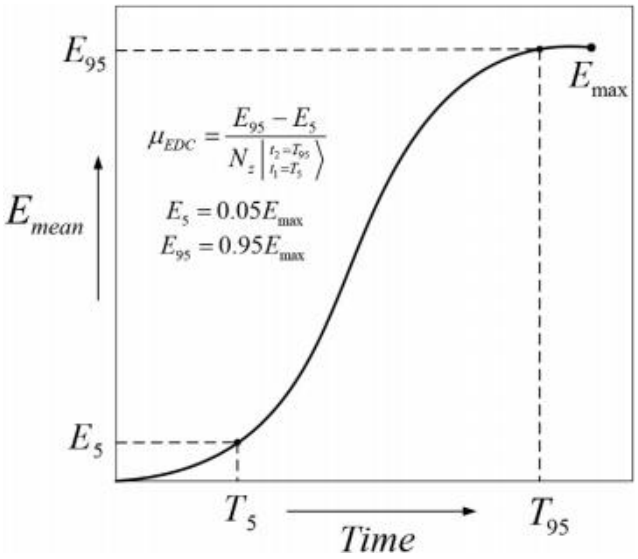

Fig. 12. Mean hysteresis energy dissipated per cycle.

Table 9
Comparison of mean hysteresis energy per cycle, $\mathbb{m}_{EDC}$ (KN.m).

Ground Motion		E_5	T_5 (sec)	E_{95}	T_{95} (sec)	N_Z	$\mathbb{m}_{EDC}$
LPGMs	Real	903.315	67.74	17,203.773	237.44	103	158.257
	Simulated	905.641	64.20	17,188.090	232.29	103	158.082
SPGMs	Real	526.262	39.36	9,995.239	214.02	121	78.256
	Simulated	536.731	33.93	10,200.810	224.10	119	81.211

response is more dominated by LPGMs, thus pushing us to acknowledge the influence of the low-frequency part of the ground motions on the total response. In addition, the mean energy dissipation per cycle $\mathbb{m}_{EDC}$ of LPGMs is 48% greater than that of SPGMs; and (3) regarding simulated ground motions, the overall response is similar to the real records; however, the isolator displacement increased by 5% and decreased by 2.5% relative to the real SPGMs and LPGMs. The base shear values are relatively estimated as being 4.4% more and 2.3% less for SPGMs and LPGMs, respectively. The maximum simulated mean hysteresis energy $\mathbb{m}_E$ of SPGMs is 2.02% higher, whereas for LPGMs it is 0.1% lower. Moreover, the simulated $\mathbb{m}_{EDC}$ values are 3.64% greater and 0.1% lower for SP and LPGMs, respectively. The controlled precision e_t is within 10~15%; therefore, the given results justify the efficiency of the ground motion generation technique.

In closing, the amount of difference in the structural response is influenced by the spectral precision achieved when the selection of SPGMs and LPGMs is in Band 2 (i.e., corresponding to the first natural period of vibration). Thus, for other cases it can be inferred that differences in response may be significant, but cannot be controlled. Also, the current seismic code provisions are suitable for the already anticipated SPGMs; however, for LPGMs, improvement is paramount for the safe design of base-isolated NRCBs and other nuclear-related structures.

Acknowledgments

This work was supported by the Nuclear power Core Technology Development Program of the Korea Institute of Energy Technology Evaluation and Planning (KETEP) grant financial resource (Number 2014151010170A). The authors would like to express their appreciation for the financial support.

References

[1] G.R. Toro, N.A. Abrahamson, J.F. Schneider, Model of strong motions from earthquakes in central and eastern North America: best estimates and uncertainties, Seismol. Res. Lett. 68 (1997) 41e57.
[2] I. Takewaki, Preliminary report of the 2011 off the Pacific Coast of Tohoku Earthquake, J. Zhejiang Univ. Sci. A (Appl. Phys. Eng.) 12 (2011) 327e334.
[3] I. Takewaki, S. Murakami, K. Fujita, S. Yoshitomi, M. Tsuji, The 2011 off the Pacific Coast of Tohoku earthquake and response of high-rise buildings under long-period ground motions, Soil Dyn. Earthq. Eng. 31 (2011) 1511e1528.
[4] T. Furumura, S. Takemura, S. Noguchi, T. Takemoto, T. Maeda, K. Iwai, S. Padhy, Strong ground motions from the 2011 off-the Pacific-Coast-of-Tohoku, Japan (Mw=9.0) earthquake obtained from a dense nationwide seismic network, Landslides 8 (2011) 333e338.
[5] A. Ali, N. Abu Hayah, D. Kim, S.G. Cho, Probabilistic seismic assessment of base-isolated NPPs subjected to strong ground motions of Tohoku Earthquake, Nucl. Eng. Technol. 46 (2014) 699e706.
[6] Y. Araki, M. Kim, S. Okayama, K. Ikago, K. Uetani, Dynamic instability in high-rise SMRFs subjected to long-period ground motions, World Acad. Sci. Eng. Technol. 59 (2011) 2496e2503.
[7] Z. Xiang, Y. Li, Statistical characteristics of long period response spectra of earthquake ground motion, in: 12th World Conference on Earthquake Engineering, 2000. Auckland, New Zealand, 12WCEE, January.
[8] F. Naeim, The Seismic Design Handbook, second ed., Springer, Los Angeles, CA, USA, 2000, pp. 723e756.
[9] F. Naeim, J.M. Kelly, Design of Seismic Isolated Structures: From Theory to Practice, John Wiley and Sons, Inc., New York, USA, 1999, pp. 63e76.
[10] I.D. Guptaa, M.D. Trifunac, A note on the nonstationarity of seismic response of structures, Eng. Struct. 22 (2000) 1567e1577.
[11] Y. Dong, Y. Li, M. Xiao, M. Lai, Unscented Kalman filter for time varying spectral analysis of earthquake ground motions, Appl. Math. Model. 33 (2009) 398e412.
[12] J.P. Conte, K.S. Pister, S.A. Mahin, Nonstationary ARMA modelling of seismic motions, Soil Dyn. Earthq. Eng. 11 (1992) 411e426.
[13] Y. Dong, S. Ji, M. Xiao, Simulation of ground motions using time varying vector ARMA model, in: 13th World Conference on Earthquake Engineering, 2004. Vancouver, Canada, 13WCEE.
[14] Y. Dong, Application of ARMA model for simulation of ground motions and spectra estimation (in Chinese) Thesis for master degree, Chongqing Jianzhu University, Chongqing, 2000.
[15] A.A. Mobarakeh, F.R. Rofooei, G. Ahamdi, Simulation of earthquake records using time-varying Arma (2, 1) model, Probab. Eng. Mech. 17 (2002) 15e34.
[16] T.H.D. Popescu, S. Demetriu, Analysis and simulation of strong earthquake ground motions using ARMA models, Automatica 26 (1990) 721e737.
[17] F. McKenna, G.L. Fenves, OpenSees, the Open System for Earthquake Engineering Simulation, Pacific Earthquake Engineering Research (PEER) Center, University of California, Berkeley, USA, 2001 [Internet]. Available from: http://opensees.berkeley.edu.
[18] N.H. Lee, K.B. Song, Seismic capacity evaluation of the prestressed/reinforced concrete containment, Young-Gwang nuclear power plant units 5 & 6, Nucl. Eng. Des 192 (1992) 189e203.
[19] Korea Testing & Research Institute, Lead rubber bearing (LRB) performance evaluation, KTIR (2011), 11-TBS-140.
[20] International Standard, Elastomeric seismic-protection, Part 1: Test methods, ISO 22762:2010, 6.2.2, 2010, pp. 20e26. Geneva, Switzerland.
[21] Regulatory Guide 1.60, Design Response Spectra for Seismic Design of Nuclear Power Plants, U.S. Nuclear Regulatory Commission, Washington, DC, 1973.
[22] E.I. Katsanos, A.G. Sextos, G.D. Manolis, Scaling of earthquake ground motion records: A state-of-the-art review from a structural engineering perspective, Soil Dyn. Earthq. Eng. 30 (2010) 157e169.
[23] American Society of Civil Engineers, Minimum Design Loads for Buildings and Other Structures, ASCE Standard (no. 007e05), 2006.
[24] C. Haselton, J.W. Baker, Ground motion intensity measures for collapse capacity prediction: choice of optimal spectral period and effect of spectral shape, in: Proceeding, 8th National Conference on Earthquake Engineering, 2006. San Francisco, CA, 10 p.
[25] P. Yang, Y.M. Li, M. Lai, A new method for selecting input waves for time history analysis, China Civil Eng. J. 33 (2000) 33e37.
[26] N.N. Ambraseys, J. Douglas, D. Rinaldis, C. Berge-Thierry, P. Suhadolc, G. Costa, R. Sigbjornsson, P. Smit, Dissemination of European strong-motion data, in: CD-ROM Collection vol. 2, Engineering and Physical Sciences Research Council, UK, 2004.
[27] American Society of Civil Engineers, Seismic analysis of safety-related nuclear structures and commentary, ASCE Standard (no. 004e098), 2000.
[28] J. Iyama, H. Kuwamura, Application of wavelets to analysis and simulation of earthquake motions, Earthq. Eng. Struct. Dyn. 28 (1999) 255e272.
[29] A. Heidari, E. Salajegheh, Time history analysis of structures for earthquake loading by wavelet networks, Asian J. Civil Eng. 7 (2006) 155e168.
[30] A. Heidari, E. Salajegheh, Wavelet analysis for processing of earthquake records, Asian J. Civil Eng. 9 (2008) 513e524.

[31] Y. Grenier, Time-dependent ARMA modeling of nonstationary signals, IEEE Trans. Acoust. Speech Signal Process 31 (1983) 899e911.
[32] F. Kozin, ARMA models of earthquake records, Probab. Eng. Mech. 3 (1988) 58e63.
[33] H. Akaike, A new look at the statistical model identification, IEEE Trans. Autom. Contr. 19 (1974) 716e723.
[34] H. Akaike, Use of statistical models for time series analysis, in: Proceedings of IEEE ICASSP86, 1986, pp. 3147e3155. Tokyo.
[35] J.D. Hamilton, Handbook of Econometrics 4, Elsevier Science B.V., 1994, pp. 3039e3080.
[36] R.W. Clough, J. Penzien, Dynamics of Structures, Third edition, Computer & Structures, Inc., Berkeley, CA 94704, USA, 2003, pp. 234e244.
[37] F. Alemdar, A.E. Ulku, Y. Bulut, J.C. Hays, N. Vaidya, High frequency cut off analysis for reactor equipment, in: Transactions, SMiRT 21, paper # 435, 2011. New Delhi, India.